Instantaneous Normal Modes and Cooperative Dynamics in a Quasi-Two-Dimensional System of Particles†

Ronen Zangi

Department of Biophysical Chemistry, University of Groningen, Nijenborgh 4, 9747 AG Groningen, The Netherlands

Stuart A. Rice*

Department of Chemistry and The James Franck Institute, The University of Chicago, Chicago, Illinois 60637

Received: December 2, 2003; In Final Form: February 10, 2004

In recent molecular dynamics simulations [*Phys. Rev. E* **2003**, *68*, 061508] we found that the deviation of the single-particle displacement distribution from Gaussian form is a characteristic that is common to all phases of a system confined to a quasi-two-dimensional geometry (liquid, hexatic, and solid). These deviations, which intensify with increasing density and/or decreasing temperature, are a consequence of correlated particle motion and are related to the emergence of a third dynamical relaxation mode in the intermediate time regime. It was suggested that this collective motion is generated by superpositions of instantaneous normal mode vibrations along diffusive paths. The diffusive paths are along the directions with strong bond-orientation correlation and start to grow in amplitude rapidly on entry into the hexatic phase. In this paper we report the results of a study of the relation between the distribution of the instantaneous normal mode frequencies and the observed cooperative dynamics. We find that as the temperature decreases the distribution of the instantaneous normal mode frequencies (the real and the imaginary parts) shifts to lower frequency and the deviations of the single-particle displacement distribution from Gaussian form increase. The results indicate that there is a relationship between the average time at which the cooperative dynamics of the system is maximum, $\langle t_{max} \rangle$, and the average value of the squared frequency for which the spectrum of the imaginary normal modes is maximum, $\langle -\omega^2_{max} \rangle$, that has the form $\ln \langle t_{max} \rangle = \ln \langle -\omega^2_{max} \rangle^{-1} + c(\rho)$, where $c(\rho)$ is a density dependent constant.

I. Introduction

Single-particle motion in a condensed phase is affected by interactions with many other particles. However, at short and long times, the many-body problem simplifies and the one-body dynamics are deterministic and stochastic, respectively, in those time regimes. As a result, the distribution of the single-particle displacement in each of these two limiting time regimes has a Gaussian form. Deviations from the Gaussian distribution of particle displacements that occur at intermediate times in three-dimensional systems are very small.[1−3] In these cases, the first correction to the Gaussian approximation is typically 10% or less of the leading term and successive terms are even smaller. However, stronger deviations from Gaussian behavior have been observed in dense glass-forming liquids just above the glass transition.[4−7]

The situation in two dimensions is different. It has been shown, both computationally[8−11] and experimentally,[12,13] that the motion of dense two-dimensional liquids is heterogeneous, and the single-particle displacement distribution has a large non-Gaussian component. Moreover, it is found that in these dense liquids the single-particle displacement involves cooperative stringlike motions in some time regimes. Recently, it was also found that the density dependence of the deviations from a Gaussian form exhibits a sharp increase in its magnitude at the liquidus density and extends into the hexatic and crystalline phases.[14,15] For densities greater than the liquidus density, three dynamical relaxation processes were observed that include, at intermediate times, a slowing down in the rate of growth of the diffusive displacement of a particle due to the cage effect. As the density increases toward the solidus density, the dependence of the mean squared displacement on time, at intermediate times, changes from sublinear to zero. The onset of the long time relaxation mode corresponds to the time at which the deviation of the particle displacement distribution from Gaussian form is a maximum. At this time, which increases exponentially with the density, the self-part of the van Hove function exhibits multiple maxima with respect to r while the distinct-part of the van Hove function is a maximum at the origin, thereby signaling jump dynamics. At long times the particle mean square displacement has diffusive character at all densities, including solid phase densities. The continuity of the character of the particle displacement from the liquid phase, through the hexatic phase, into the solid phase is striking and suggests that it arises from the same physical phenomenon. It has been argued that the drivers for the collective motions are superpositions of instantaneous normal mode vibrations along paths that feature activated hopping of particles. These diffusive paths are along the directions with strong bond-orientation correlation.[14,15]

Normal mode analysis of the motion of a many-body system is rigorously possible in crystals for which the restoring forces

† Part of the special issue "Hans C. Andersen Festschrift".

10.1021/jp031283v CCC: $27.50
Published on Web 04/02/2004

acting on a particle are linear in the displacement of the particle from its equilibrium position.[16] The analysis is generated by expanding the total potential energy of the system, U, to second order (harmonic approximation) in the deviation, δ, of the set of atomic coordinates $\mathbf{r} \equiv \{r_1, ..., r_N\}$ from their lattice sites $\mathbf{r}_0$:

$$U(\mathbf{r}) = U(\mathbf{r}_0) + \mathbf{F}(\mathbf{r}_0)\delta + {}^1/_2\mathbf{G}(\mathbf{r}_0)\delta^2 \quad (1)$$

Assuming the lattice configuration is a minimum of U, the linear term $\mathbf{F}(\mathbf{r}_0)$ vanishes. The second-order term is the force-constant matrix $\mathbf{G}$, namely, the second derivatives of the potential energy with respect to the mass-weighted coordinates (the dynamical matrix). Its eigenvalues are the squares of the vibrational frequencies of the system, ω, from which the density of states, $\rho(\omega)$, can be calculated. The eigenfunctions of the dynamical matrix are the normal modes of vibration (phonons).

In a liquid there exist no well-defined lattice sites, and most configurations will not be minima of the potential (i.e., they have no unique position of mechanical stability about which the potential energy of the system can be expanded). Nevertheless, Zwanzig has argued that collective variables, analogous to longitudinal and transverse phonons in crystals, do exist in classical liquids.[17] He noted, however, that their lifetimes are exceedingly short except in the glassy state. The application of normal mode analysis to the liquid state will, therefore, generate a fraction of negative eigenvalues corresponding to imaginary frequencies. Imaginary frequencies are a signature of negative curvature of the potential energy surface and are a measure of barrier or saddle point crossing. Thus, the imaginary normal modes reflect the fluidity of the system. The states that are associated with the negative eigenvalues are termed unstable modes while those associated with the positive eigenvalues are termed stable modes. The density of states is, therefore, the sum of two physically distinct parts

$$\langle\rho(\omega)\rangle = \langle\rho_s(\omega)\rangle + \langle\rho_u(\omega)\rangle \quad (2)$$

The temperature dependence of the distribution of imaginary frequencies has been studied extensively.[18,19]

The justification for using a harmonic analysis in liquids is to be found in the restriction of that analysis to short times. According to the Maxwell description of viscoelasticity, for short times a liquid behaves like a solid and the stable modes give the distribution of frequencies for particle displacements relative to the corresponding averaged lattice. The lattice is not stable, however, and rearranges. This rearrangement is governed by the unstable modes. This idea has been followed up by many authors,[20−25] most notably by Keyes and co-workers[26−28] and by Stratt and co-workers[29−31] via the definition of instantaneous normal modes of a liquid.

In the activated view of transport, the dynamics of the system is viewed as a series of barrier crossings on the multidimensional free energy surface. Goldstein has exploited this viewpoint in a discussion of the approach to the glass transition.[32] The hopping rate between local minima was identified as the crucial quantity in a theory of self-diffusion.[33] It is argued that the imaginary frequency distribution of the instantaneous normal modes yields considerable information about the energy barriers to diffusion.[34−36] In particular, a correlation between the fraction of unstable normal modes and the self-diffusion constant has been observed.[23,37,38] However, imaginary normal modes frequencies have been found to exist in glass-forming liquids below the glass transition.[25,39−42] These nondiffusive unstable normal modes were associated with "potential shoulder" motions that correspond to negative curvature inside a single well while the diffusive unstable normal modes were associated with "double well" motions that correspond to barrier crossing. It should be noted that diffusion constants are descriptions of the particle motion in the long time regime, whereas the instantaneous normal modes have utility only in the short time regime. Nevertheless, it turns out that there is enough information in the instantaneous normal mode spectrum to cast light on the (long time) dynamics of the system.[43]

In this study, we investigate the relation between the distribution of the instantaneous normal mode frequencies and the observed cooperative dynamics in a quasi-two-dimensional assembly of particles. Our goal is the establishment of a one-to-one relationship between the character of the instantaneous normal mode spectrum and the observed behavior of the mean squared single-particle displacement as a function of time and density; we do not attempt to calculate the diffusion constant. We find that as the temperature decreases the distribution of the instantaneous normal mode frequencies (the real and the imaginary parts) shifts to lower frequency and the deviations of the single-particle displacement distribution from Gaussian form increase. Our results indicate that the relation between the average time at which the cooperative dynamics of the system is maximum, $\langle t_{max}\rangle$, and the average value of the squared frequency for which the spectrum of the imaginary normal modes is maximum, $\langle -\omega^2_{max}\rangle$, has the form $\ln\langle t_{max}\rangle = \ln\langle -\omega^2_{max}\rangle^{-1} + c(\rho)$, where $c(\rho)$ is a density dependent constant.

II. Methods

The model systems that we study consist of a single layer, with $N = 2016$ particles, placed in a quasi-two-dimensional simulation box. The simulation box is rectangular in the xy-plane, with side lengths in the ratio $x/y = 7/(8\sqrt{3}/2)$; it has a height slightly greater than the particle diameter (see below). Periodic boundary conditions were imposed in the x and y directions, but not in the z direction. The calculations were carried out, and the results are reported below, in terms of the reduced variables $r^* = r/\sigma$, $z^* = z/\sigma$, $T^* = k_BT/\epsilon$, $\rho^* = \rho\sigma^2$, $t^* = t(k_BT/m\sigma^2)^{1/2}$, $\omega^* = \omega(k_BT/m\sigma^2)^{-1/2}$, $m = 1$, with σ the diameter of the particle, ρ the number density, m the mass of the particle, t the time, ω a normal mode frequency, and 3.689ϵ the value of the interparticle potential at $r^* = 1.000$. Although the particles can move in the z direction under the influence of a z-dependent one-body potential, we choose to characterize the state of the system with the two-dimensional number density $\rho = N/A$, where A is the area of the of the simulation cell in the xy-plane, since the height of the cell, H, is constant in all of the simulations presented in this paper. The same number of particles was present in the simulation cell for all of the densities studied. To study the properties of the system with different particle densities, we changed the area of the simulation cell in the xy-plane. The forms of the pair potential and the confinement potential were chosen to model an assembly of constrained colloid particles, since extensive experimental data are available for the single-particle mean squared displacement as a function of time and density for this system (see section IV).

The interparticle potential was represented by

$$u(r^*) = A\left(r^* - \frac{1}{2}\right)^{-\alpha} \quad (3)$$

with $A = 2 \times 10^{-19}$ and $\alpha = 64$. The functional form in eq 3 is hard-core repulsion but has continuous derivatives. It is plotted

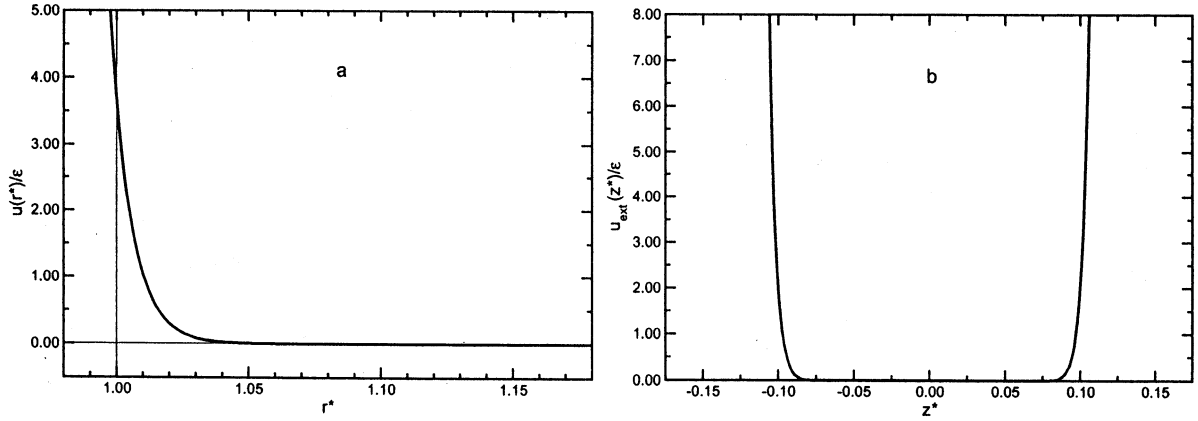

Figure 1. (a) The pair potential used in this study. (b) The external potential confining the particles to a slab with height of $H = 1.20\sigma$. The external potential is plotted as a function of the reduced center of mass coordinate along the vertical axis (z-axis) measured from the center of the cell.

in Figure la. The confinement of the particles in the $\pm z$ directions is affected by the action of a one-body z-dependent external field. Different forms can be chosen for this field, the simplest being that for hard parallel walls. Then the extra degree of freedom that is introduced in the thermodynamic description of the system is the spacing between those two walls. The shape of the potential that was chosen

$$u_{\text{ext}}(z^*) = D\epsilon(z^*)^{\zeta} \tag{4}$$

is such as to confine the system to form a slab with well-specified height H. In eq 4, z^* is the distance from the center of the cell to the center of mass of the particle and $\zeta = 24$, $D = 2 \times 10^{24}$; this potential confines the particles as if they were in a cell with an effective height of $H = 1.20\sigma$ (i.e., $z^* = \pm 0.10$) and is shown in Figure lb. The slab height is small enough so that the buckled phase is unstable even at the highest two-dimensional number density studied ($\rho^* = 1.120$), and the transverse density distribution is homogeneous.[44]

The molecular dynamics (MD) simulations were carried out in the microcanonical ensemble using the "velocity Verlet" algorithm.[45,46] The distance at which the potential was cut off was 1.5σ and the time step used was, in reduced units, 5×10^{-4}; the associated rms fluctuation in total energy did not exceed one part in 10^5.

The initial configurations for the simulations at $T^* = 1.0000$ were taken from equilibrated configurations of a previous study that investigated the correlated motion of the particles.[14] The system was further equilibrated for 1.2×10^6 MD steps. The simulations at $T^* = 1.0000$ were performed for eight densities in the range $0.740 \le \rho^* \le 1.120$ that covers the liquid, hexatic, and solid phases. For four densities, $\rho^* = 0.740$, 0.820, 0.880, and 1.120, the behavior of the system at four other different temperatures, $T^* = 0.1000$, 0.0100, 0.0010, and 0.0001, was studied as well. At each density the required temperature was created in a preequilibration stage by multiplying the velocities, every 1×10^5 MD steps, by an appropriate constant. This stage was repeated until the relative difference between the average temperature of the system and the prescribed temperature did not exceed 5×10^{-4} in reduced units. Then the system was further equilibrated for 1.2×10^6 time steps as for the case at $T^* = 1.0000$. The equilibration and the data collection stage were carried out without velocity rescaling (thus, in the microcanonical ensemble) to ensure uninterrupted dynamical paths. Nevertheless, the relative rms deviation of the average temperature from the prescribed temperature was less than 5×10^{-4}.

The lateral pressure, P_l, was calculated from

$$P_l = \frac{Nk_BT + \langle W_l \rangle}{V} \tag{5}$$

where the angular brackets indicate an average value, the volume, V, is $V = AH$ and the lateral virial, W_l, is

$$W_l = -\frac{1}{2}\sum_{i=1}^{N}\sum_{j>i}^{N}\frac{x_{ij}^2 + y_{ij}^2}{r_{ij}}\frac{\partial u(r)}{\partial r}\bigg|_{r=r_{ij}} \tag{6}$$

The structural properties of the system were characterized by calculating the radial distribution function, $g(r_{xy})$

$$g(r_{xy}) = \frac{A}{2\pi r_{xy} N(N-1)}\left\langle \sum_{i=1}^{N}\sum_{j\neq i}^{N}\delta(\mathbf{r}_{\mathbf{xy},i} - \mathbf{r}_{\mathbf{xy},j}|)\right\rangle \tag{7}$$

where $\mathbf{r}_{\mathbf{xy}}$ is the lateral vector component of the particle's position, and the bond-orientation function, $G_6(r_{xy})$

$$G_6(r_{xy}) = \langle \psi_6^*(0)\psi_6(r_{xy})\rangle \tag{8}$$

where $\psi_6(r_{xy})$ is the local order parameter descriptive of the hexagonal symmetry characteristic of close-packing in two dimensions; it is defined by

$$\psi_{6i} = \frac{1}{n_i}\sum_{j=1}^{n_i} e^{i6\theta_{ij}} \tag{9}$$

The sum in eq 9 is taken over the n_i nearest neighbors to particle i, as determined by a two-dimensional Voronoi polygon construction.[47] We denote by θ_{ij} the angle between the vector $\mathbf{r}_{\mathbf{xy},ij}$ and an arbitrary fixed axis. The global translational order parameter is defined to be the sum of the Fourier components of the density

$$\Phi_T = \frac{1}{N}\sum_{i=1}^{N} e^{i\vec{G}\cdot\vec{r}_i} \tag{10}$$

where $\vec{G}$ is a reciprocal lattice vector of the triangular two-dimensional lattice. The corresponding global orientational order parameter is defined by

$$\Phi_6 = \frac{1}{N}\sum_{i=1}^{N}\psi_{6i} \tag{11}$$

The lateral mean square displacement, $\Delta r_{xy}^2(t)$, was calculated using the following expression

$$\langle \Delta r_{xy}^2(t) \rangle = \frac{1}{N}\sum_{i=1}^{N}[\mathbf{r_{xy}}(t) - \mathbf{r_{xy}}(0)]^2 \tag{12}$$

We describe the time dependent deviation of the particle displacement from Gaussian behavior by the non-Gaussian parameter, $\alpha_2(t)$. In two dimensions it has the following representation:

$$\alpha_2(t) = \frac{\langle [\mathbf{r_{xy}}(t) - \mathbf{r_{xy}}(0)]^4 \rangle}{2\langle [\mathbf{r_{xy}}(t) - \mathbf{r_{xy}}(0)]^2 \rangle^2} - 1 \tag{13}$$

The calculation of the in-plane instantaneous normal mode frequencies was carried out by evaluating the $2N \times 2N$ force-constant matrix from the second derivatives of the potential energy function with respect to the particle's coordinates. Then the force-constant matrix was diagonalized yielding $2N$ eigenvalues. These eigenvalues are the squares of the $2N$ normal modes frequencies ω. The second derivatives of the interparticle potential, $u(r)$, are calculated from the following expressions:

$$\frac{\partial^2 u(r)}{\partial x_i \partial y_i} = -\frac{x_{ij}y_{ij}}{r_{ij}^2}\left[\frac{\partial^2 u(r)}{\partial r^2}\bigg|_{r=r_{ij}} - \frac{1}{r_{ij}}\frac{\partial u(r)}{\partial r}\bigg|_{r=r_{ij}}\right] \tag{14}$$

$$\frac{\partial^2 u(r)}{\partial x_i \partial x_j} = -\frac{1}{r_{ij}^2}\left[x_{ij}^2\frac{\partial^2 u(r)}{\partial r^2}\bigg|_{r=r_{ij}} + \frac{y_{ij}^2}{r_{ij}}\frac{\partial u(r)}{\partial r}\bigg|_{r=r_{ij}}\right] \tag{15}$$

$$\frac{\partial^2 u(r)}{\partial x_i \partial y_i} = -\sum_{j\neq i}^{N}\frac{\partial^2 u(r)}{\partial x_i \partial y_i} \tag{16}$$

$$\frac{\partial^2 u(r)}{\partial x_i \partial x_i} = -\sum_{j\neq i}^{N}\frac{\partial^2 u(r)}{\partial x_i \partial x_i} \tag{17}$$

All the calculations were carried out with double precision so that the difference of the character of the force-constant matrix before and after the diagonalization was approximately one part in 10^{15}. The eigenvalues were averaged over 400 configurations separated by 1000 MD steps from each other.

III. Results

The thermodynamic behavior as a function of the two-dimensional number density of a system with the pair potential shown in Figure la, and of systems with other pair potentials, have been reported previously.[14,44] The plateau region (or weak van der Waals loop) observed in the lateral pressure density isotherm (Figure 2a) for the density range $0.865 \leq \rho^* \leq 0.895$ is the signature of a first-order phase transition. Figure 2b displays the global translational and orientation order parameters as a function of density. From these plots we conclude that for densities $\rho^* \leq 0.860$ the system is in the liquid phase, for densities $0.870 \leq \rho^* \leq 0.890$ it is in the hexatic phase, while for densities $\rho^* \geq 0.900$ the system is in the solid phase. These phase boundary identifications are consistent with the analysis of the pair correlation and bond-orientation correlation functions (not shown).

Figure 3 displays the fraction of the instantaneous normal modes with real and imaginary frequencies as a function of the two-dimensional number density. For densities that correspond to liquid, hexatic, and low-density solid phases, the number of

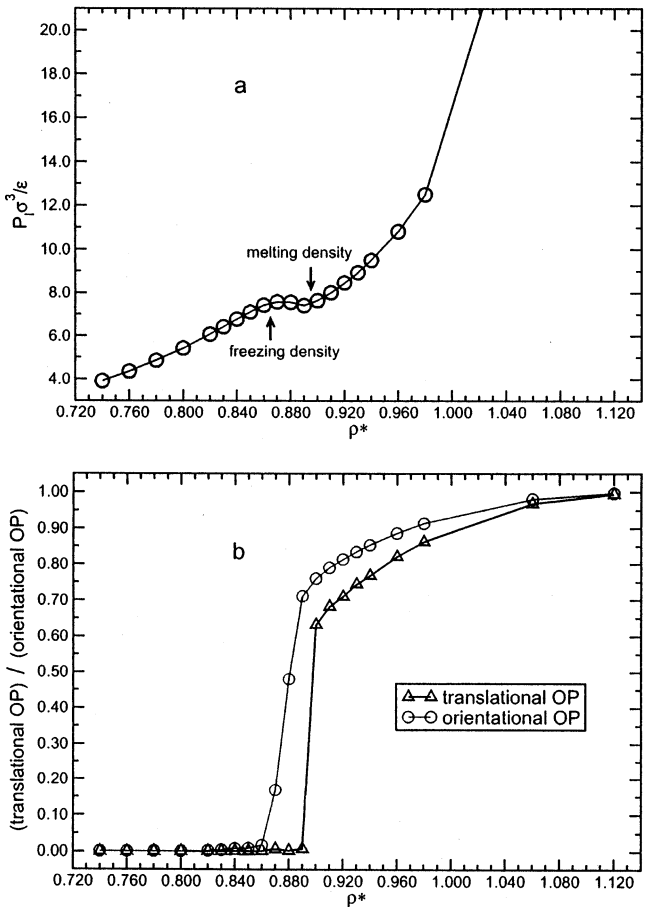

Figure 2. (a) Lateral pressure (in reduced units) as a function of the two-dimensional number density. The low-density end of the plateau region at $\rho^* = 0.865$ signifies the onset of the liquid phase while the high-density end at $\rho^* = 0.895$ marks the onset of the solid phase. (b) The global translational and orientation order parameters indicating that the hexatic phase is stable for $0.870 \leq \rho \leq 0.890$.

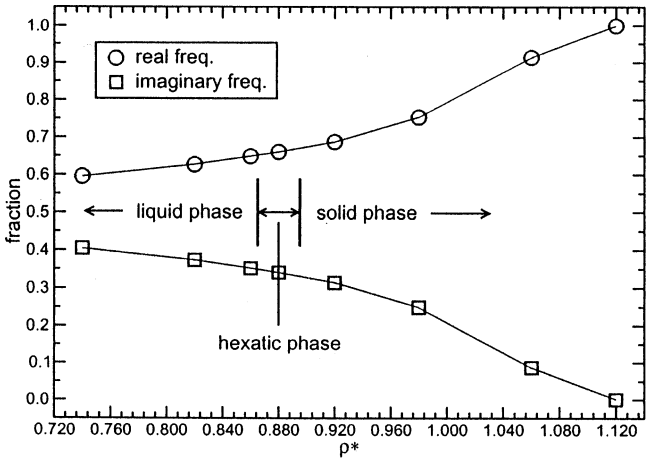

Figure 3. Fraction of the real and imaginary normal mode frequencies as a function of the two-dimensional number density for $T^* = 1.0000$. The density range of the liquid, hexatic, and solid phases is indicated.

the imaginary frequencies is large (0.40−0.32). Only at higher densities, inside the solid phase ($\rho^* \sim 0.980$), does the number of the negative eigenvalues decrease sharply to zero. At $\rho^* = 1.120$ the values of $2N - 2$ mode frequencies are larger than ~1.0 while the absolute values of two normal mode's frequencies are smaller than $\sim e^{-10}$ (they are equal to zero within the machine precision). These two normal modes correspond to two center of mass translations in the xy-plane. This is of course

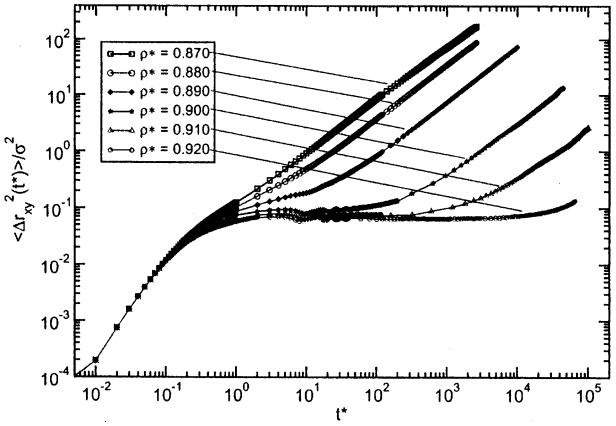

Figure 4. Lateral mean squared displacement (in reduced units) as a function of the reduced time, t^*, for two-dimensional number densities $0.870 \leq \rho^* \leq 0.920$. The curves show the emergence of the three dynamic relaxation modes. The slope of the mean squared displacement for the longest relaxation mode is linear for all densities, indicating diffusive behavior. The time of the onset of the longest relaxation mode increases exponentially with the density, and it corresponds to the time at which the deviation of the particle displacement distribution from Gaussian form is a maximum.

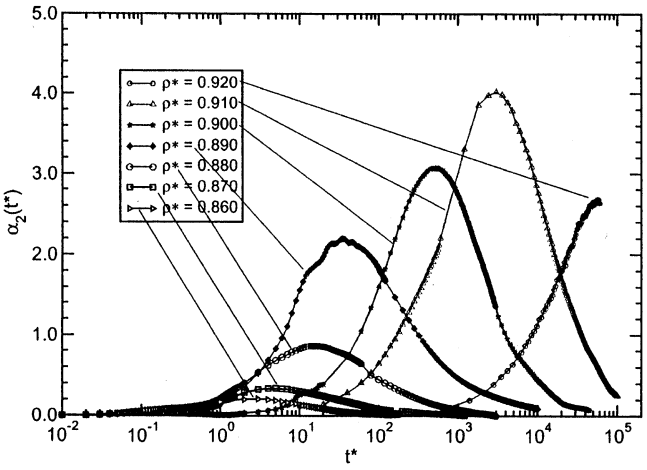

Figure 5. The non-Gaussian parameter $\alpha_2(t^*)$ as a function of the reduced time, t^*, for two-dimensional number densities $0.860 \leq \rho^* \leq 0.920$. The x-axis is plotted on a logarithmic scale. The value of $\alpha_2(t^*)$ at the maximum as well as the time at which the maximum appears increase for higher densities. The latter depend exponentially on the density.

true for every density. Note that, due to the type of periodic boundary conditions used, rotation of the center of mass around the z-axis is not possible; hence, the angular momentum is not conserved in this system.

The high fraction of imaginary instantaneous normal modes found in the liquid, hexatic, and low-density solid phases correlates with the long time diffusive behavior found for these phases. Figure 4 displays the single-particle mean squared displacement for the density range $0.870 \leq \rho^* \leq 0.920$ that corresponds to hexatic and solid phases. The plots exhibit three dynamical relaxation processes. At long times the particle mean square displacement has diffusive character (i.e., the dependence of the mean squared displacement on time is linear) at all densities shown. The time at which there is an onset of the long time diffusive motion corresponds to the time at which the deviation of the single-particle displacement distribution from Gaussian form is a maximum, t^*_{max} (Figure 5). At this time, which increases exponentially with the density, the self-part of the van Hove function exhibits multiple maxima (with respect

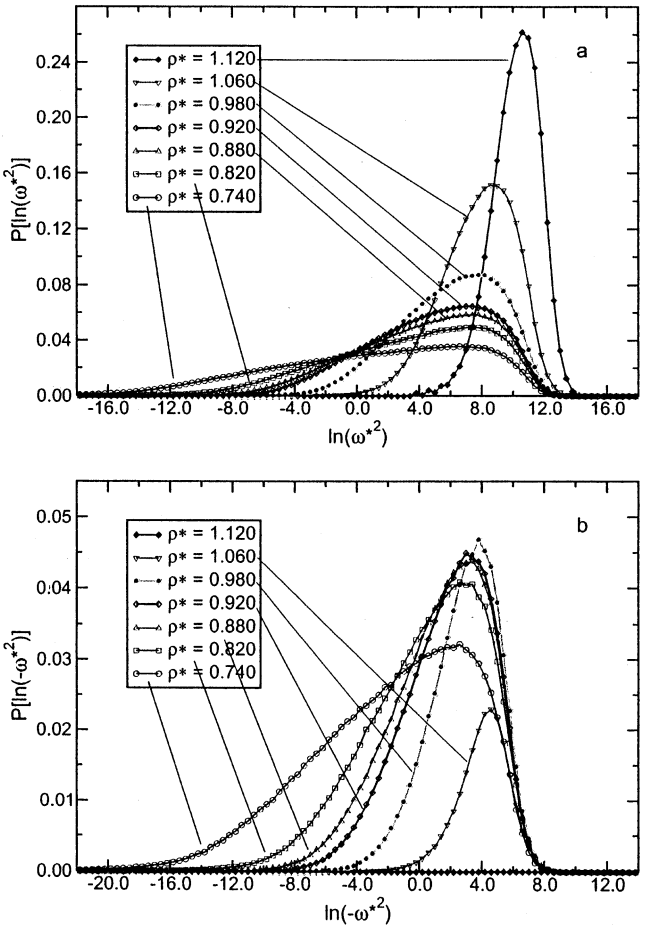

Figure 6. (a) Distribution of the natural logarithm of the positive eigenvalues (the square of the real normal mode frequencies) for two-dimensional number density in the range $0.740 \leq \rho^* \leq 1.120$ that spans the liquid, hexatic, and solid phases. (b) The distribution of the natural logarithm of the absolute value of the negative eigenvalues (the square of the imaginary normals mode frequencies). The sum of the integrals of the positive and negative eigenvalues is normalized to unity.

to the interparticle distance) while the distinct-part of the van Hove function is a maximum at the origin, thereby signaling jump dynamics.[14,15] This behavior suggests that the mechanism of diffusion involves an activated process of correlated particle hopping in random directions. As shown in Figure 3, the solid phase densities for which such diffusive behavior is observed are characterized by a substantial fraction of imaginary normal mode frequencies, implying that particles in the system easily cross barriers on the free energy hypersurface. As the fraction of imaginary normal mode frequencies decreases the probability of correlated hopping, as expressed by the time for which the diffusive behavior appears (or by t^*_{max}), decreases as well.

Figure 6a shows the distribution of the natural logarithm of the squared real normal mode frequencies for several densities. The location of the maxima for two-dimensional number densities in the range $0.740 \leq \rho^* \leq 0.920$ is the same ($\ln(\omega^{*2}) \sim 0.8$). Nevertheless, the profile is broadened toward lower frequencies as the density decreases. This density range corresponds to that for which large deviations of the single-particle displacement distribution from Gaussian form (associated with correlated motion) were observed (Figure 5). For densities $\rho^* \geq 0.980$, the locations of the maxima in Figure 6a shift toward higher frequencies and the distribution narrower as the density increases. The distributions of the imaginary normal mode frequencies are displayed in Figure 6b. Again, the width of the distribution decreases as the density increases, and for $\rho^* \geq$

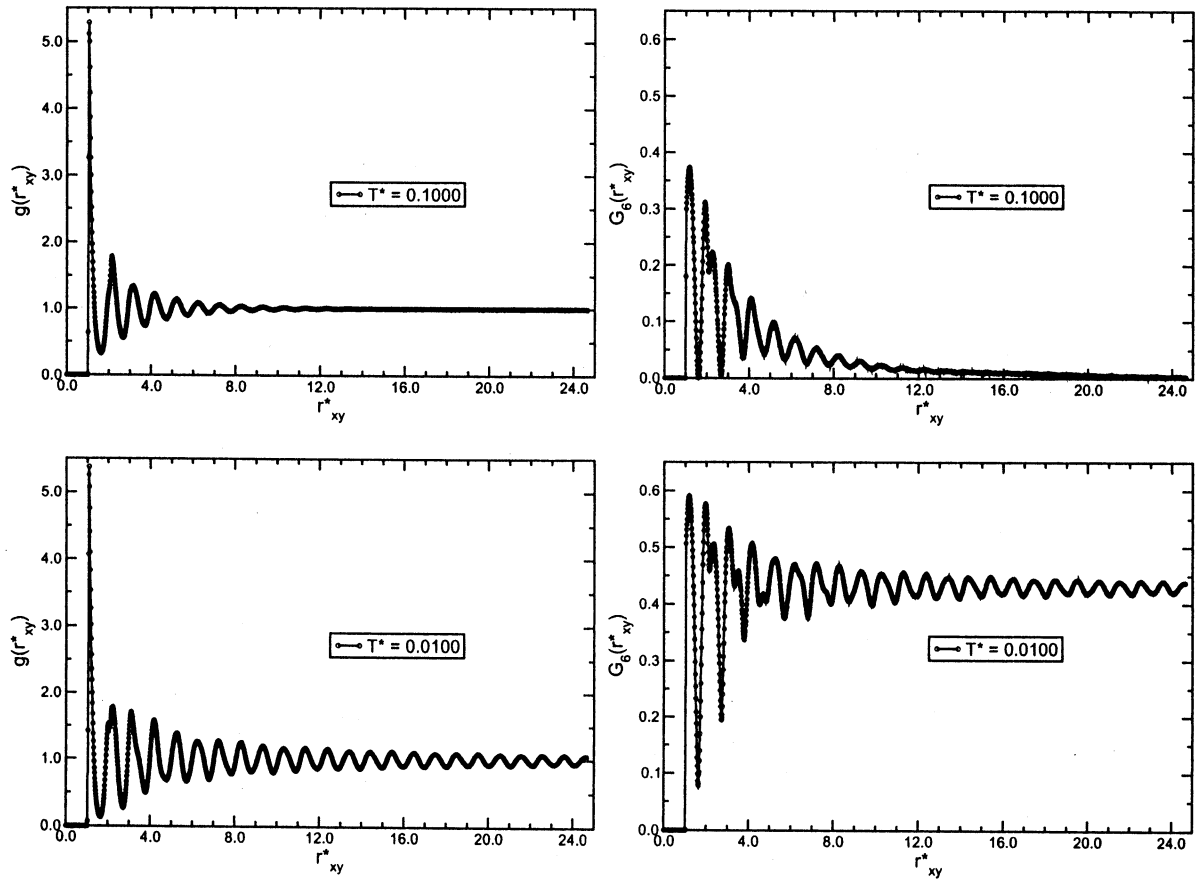

Figure 7. Pair distribution function, $g(r_{xy})$, (left panel) and the bond-orientation function, $G_6(r_{xy})$, (right panel) for $T^* = 0.1000$ and 0.0100 displaying the characteristic structural properties of the liquid and solid phases, respectively.

0.980 the maximum is shifted toward higher frequency. The number of imaginary frequencies for $\rho^* = 1.120$ is zero. All the plots of the distributions of the instantaneous normal mode frequencies are normalized such that the sum of the integrals of the real and imaginary frequencies is 1.

The fact that the distributions of the normal modes frequencies are peaked at the same location for liquid, hexatic, and low-density solid phases ($0.740 \leq \rho^* \leq 0.920$) is striking, and it differs from what is found in three-dimensional systems. Seeley and Keyes found that the maximum of the density of states of a supercooled 3D liquid shifts to higher frequency as the density increases,[37] a behavior that is observed in our two-dimensional system only for high densities, $\rho^* \geq 0.980$, where the long time diffusive behavior is not observed. It is interesting to note that for the density range $0.740 \leq \rho^* \leq 0.920$, that spans three different thermodynamic phases, there is continuity of the character of the particle displacement, namely, strong deviations from Gaussian form due to correlated motion.[14,15]

In a truly (discontinuous) hard sphere system, the thermodynamic state is temperature independent. However, the pair potential shown in Figure la contains a small region which is relatively soft. This is exploited in the present simulations to induce phase transitions, similar to those obtained by changing the two-dimensional number density, by reducing the temperature.

For four densities, $\rho^* = 0.740$, 0.820, 0.880, and 1.120, the behavior of the system at five temperatures in the range $1.0000 \leq T^* \leq 0.0001$ was studied. For $\rho^* = 0.740$ and for $\rho^* = 1.120$ the state of the system for all temperatures is liquid and solid, respectively. For $\rho^* = 0.880$ the hexatic phase at $T^* = 1.0000$ is transformed to a solid phase at $T^* = 0.1000$. The most drastic phase changes were observed for $\rho^* = 0.820$.

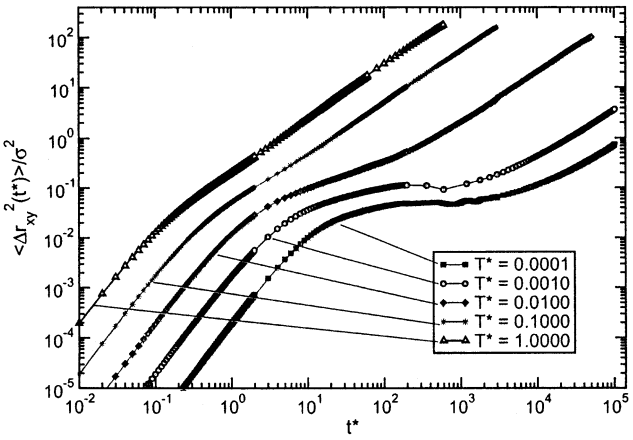

Figure 8. Lateral mean squared displacement (in reduced units) as a function of the reduced time for the temperature range $1.0000 \leq T^* \leq 0.0001$ for $\rho^* = 0.820$.

Figure 7 displays the pair correlation function and the bond-orientation correlation function for $\rho^* = 0.820$ at $T^* = 0.1000$ and 0.0100. Both correlation functions have short-range order for $T^* = 0.1000$ (liquid close to the freezing point) and long-range order for $T^* = 0.0100$ (solid close to the melting point). We predict the hexatic phase is stable in the temperature range $0.1000 > T^* > 0.0100$.

Figure 8 displays the single-particle mean squared displacement for $\rho^* = 0.820$ at five different temperatures. Similar to the results shown in Figure 4, as the temperature decreases below $T^* = 0.1000$, a new relaxation process at intermediate time emerges. The dependence of the mean squared displacement on time in this intermediate time regime is sublinear. At

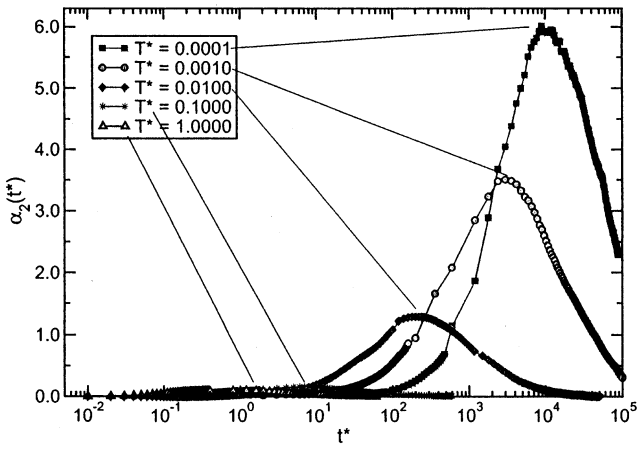

Figure 9. The non-Gaussian parameter $\alpha_2(t^*)$ as a function of the reduced time for the temperature range $1.0000 \leq T^* \leq 0.0001$ for $\rho^* = 0.820$. The location of the maximum of $\alpha_2(t^*)$ at each temperature, t^*_{max}, is indicated by the thin line. Note that the time of the onset of the longest relaxation mode of the mean squared displacement shown in Figure 8 corresponds to t^*_{max}.

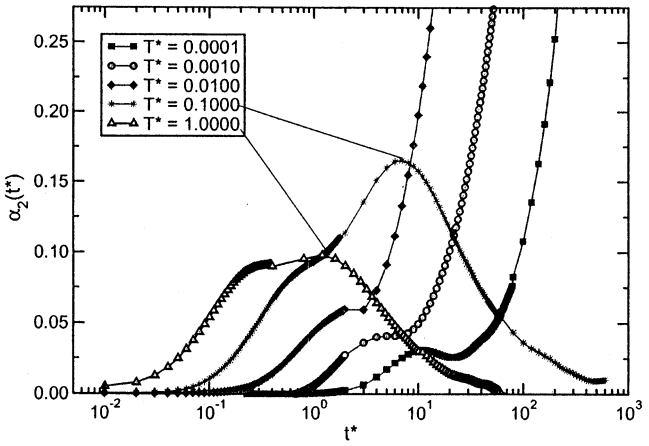

Figure 10. Magnification of Figure 9 showing the location of the maximum of $\alpha_2(t^*)$ at $T^* = 1.0000$ and 0.1000. Note that the maxima that occur at short times for all temperatures originates from the deviation of the single-particle displacement from ballistic motion due to the first collision event.

long times the particle mean square displacement has diffusive character for all temperatures including these that correspond to the solid phase. Note that although the slope of the mean squared displacement versus time at short time (describing the ballistic motion) is the same for all temperatures (since the mean squared displacement is a quadratic function of time) the intercept is temperature dependent.

In Figure 9 the value of the non-Gaussian parameter $\alpha_2(t^*)$ is plotted as a function of the reduced time for $\rho^* = 0.820$ for the temperature range $1.0000 \leq T^* \leq 0.0001$. The value of $\alpha_2(t^*)$ exhibits a maximum whose magnitude increases as the temperature decreases. The time for which $\alpha_2(t^*)$ is maximum, t^*_{max}, (indicated by thin lines in Figure 9) corresponds to the onset of long time diffusion (Figure 8). Figure 10 shows $\alpha_2(t^*)$ on a different scale indicating the location of the maxima of $\alpha_2(t^*)$ at $T^* = 1.0000$ and 0.1000. Note that the maxima that occur at short times for all temperatures originate from the deviation of the single-particle displacement from ballistic motion due to the first collision event.[14] The behavior of this maximum as a function of the temperature is opposite to that of the maximum that is due to correlated motion observed at larger time.

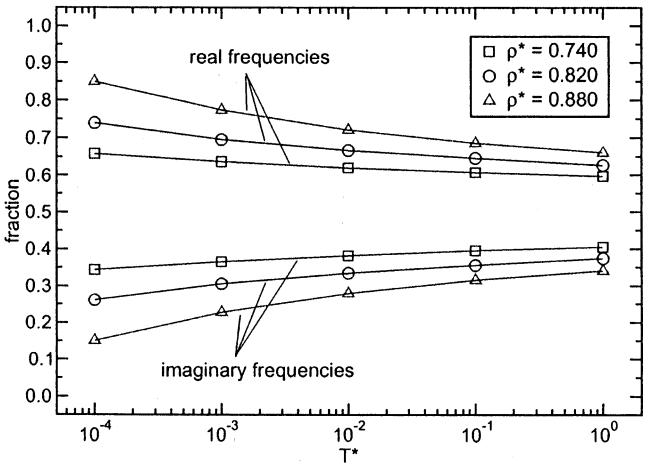

Figure 11. The fraction of the real and imaginary normal mode frequencies as a function of the temperature for $\rho^* = 0.740$, 0.820, and 0.880.

The fraction of the instantaneous normal modes with real and imaginary frequencies as a function of the temperature for three densities $\rho^* = 0.740$, 0.820, and 0.880 is displayed in Figure 11. The decrease of the imaginary normal modes frequencies with temperature decrease is small. For example, for $\rho^* = 0.820$ the fraction of the imaginary normal modes is 0.35 at $T^* = 0.1000$ (liquid) while it is 0.33 at $T^* = 0.0100$ (solid). The persistence of a large fraction of imaginary frequencies in the liquid, hexatic, and solid phases suggests similarity of the dynamical behavior (cooperative motion) found in these phases.

The distributions of the real and imaginary instantaneous normal mode frequencies for $\rho^* = 0.820$ are shown in parts a and b of Figure 12, respectively. In both cases, as the temperature decreases there is a continuous shift of the distribution toward lower frequency. The number of particles that participate in a normal mode motion increases as the frequency of the normal mode decreases; hence, it is plausible to suggest that the enhanced correlated motion observed as the temperature decreases is due to excitations of long wavelength normal modes above the free energy barrier for crossing. This argument implies a relation between t^*_{max} and the value of the real and imaginary frequency for which the corresponding spectrum of the normal modes is maximum, ω^{*2}_{max} and $-\omega^{*2}_{max}$, respectively. Figure 13 displays the value of $\ln(t^*_{max})$ as a function of $\ln(\omega^{*2}_{max})$ and $\ln(-\omega^{*2}_{max})$. Also plotted are the lines obtained from a linear regression fit. The high value of the regression coefficients (0.997 and 0.991) indicates that a linear relation between $\ln(t^*_{max})$ and $\ln(\omega^{*2}_{max})$, $\ln(-\omega^{*2}_{max})$ does exist. The value of the slope is -1.0005 and -1.0975 for the case of the real and imaginary frequencies, respectively. Since diffusion is associated with the imaginary frequencies, the relation between t^*_{max} and $-\omega^{*2}_{max}$ is of the form

$$\ln \langle t^*_{max} \rangle = \ln \langle -\omega^{*2}_{max} \rangle^{-1} + c(\rho^*) \qquad (18)$$

where $c(\rho^*)$ is a density dependent constant as is evident from Figure 5 and Figure 6 where it is shown that as the density changes, t^*_{max} changes but $-\omega^{*2}_{max}$ does not.

In Figure 14 we plot the same distributions as in Figure 12 with the squared frequencies scaled by $k_B T^*$. The resulting distributions are centered at around the same value and differ only in their width. Exactly the same behavior is observed for $\rho^* = 0.740$ and 0.880 (Figure 15). These results are similar to

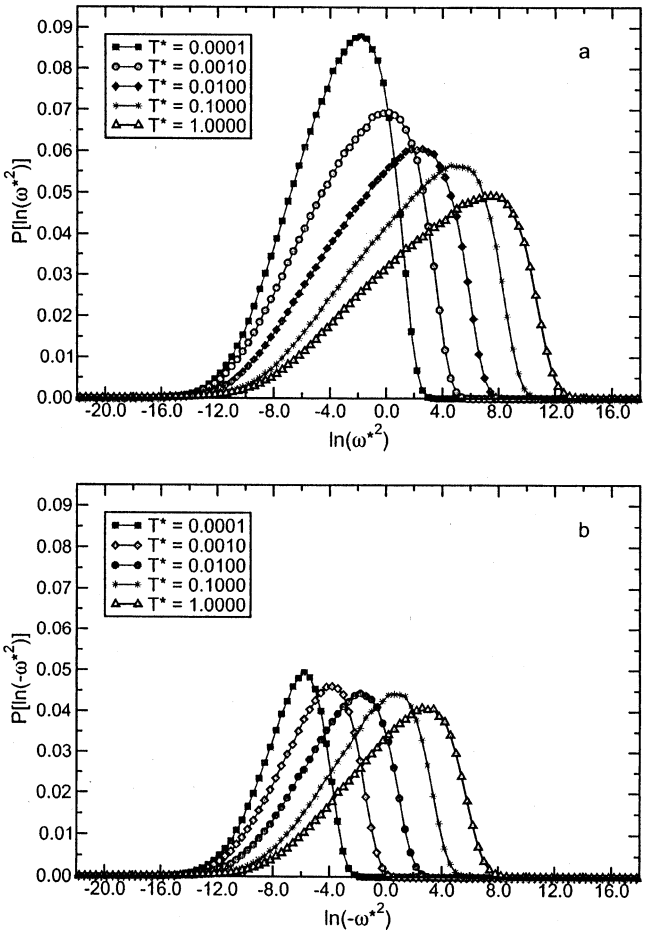

Figure 12. Distribution of the natural logarithm of the positive (a) and negative (b) eigenvalues for the temperature range $1.0000 \leq T^* \leq 0.0001$ for $\rho^* = 0.820$. The graphs show that as the temperature decreases the distributions are shifted toward lower frequencies.

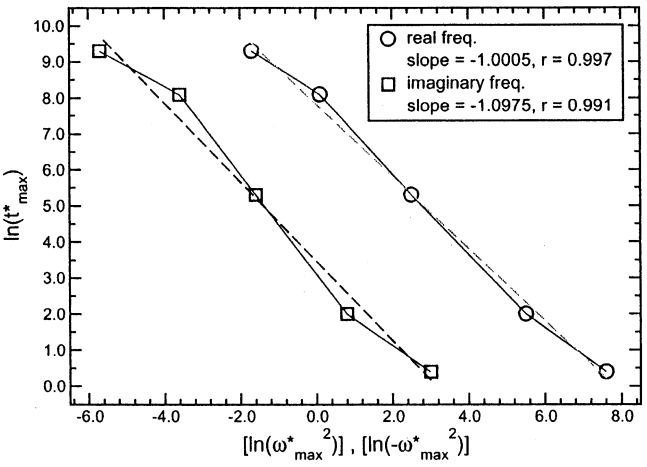

Figure 13. The time at which the deviation of the single-particle displacement from Gaussian form is maximum, t^*_{max}, as a function of the value of the real and imaginary frequency for which the corresponding density of states is maximum, ω^{*2}_{max} and $-\omega^{*2}_{max}$ respectively. The dashed lines are results obtained from a linear regression procedure.

those obtained by Keyes[18] for the temperature dependence of the imaginary frequency distribution, $\langle \rho_u(\omega; T) \rangle = a(T)\omega e^{-c\omega^4/T^2}$. However, for the solid phase at very high density, $\rho^* = 1.120$, where all the normal mode frequencies are real, we observe a different behavior. Figure 16 indicates that the distributions of the normal mode frequencies are peaked at around the same value without thermal scaling. The effect of decreasing the

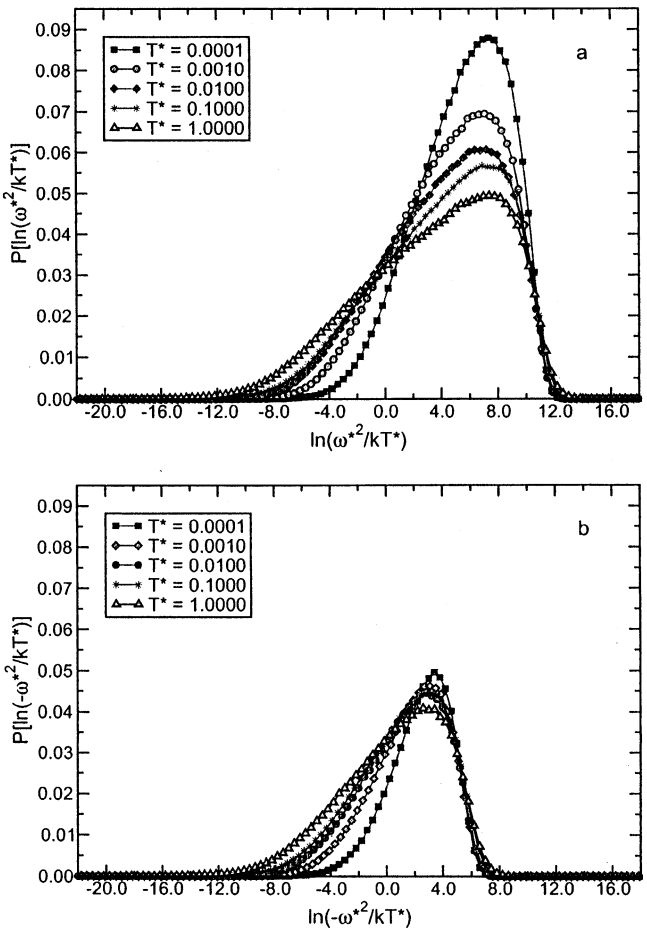

Figure 14. Same as Figure 12 but with thermal scaling of the frequencies, ω^{*2}/kT^*. The graphs show that the distributions are peaked at around the same frequency.

temperature is to yield narrower distributions that are shifted from high frequency to lower frequency.

IV. Discussion

The deviation of the single-particle displacement distribution from Gaussian form is a result of correlated motion that has also been observed in real quasi-two-dimensional colloid suspensions.[12,13] The ubiquity of this behavior in colloid and atomic systems is striking in view of the fact that the elementary particle dynamics are different for the two systems. Specifically, colloid particles exhibit Brownian motion with a self-diffusion coefficient that depends on the viscosity of the suspending medium, and their motion generates a nontrivial hydrodynamic coupling that is transmitted by the suspending medium and is concentration dependent. The appropriate equations of motion involve a complex combination of fluctuating forces due to the solvent and systematic forces due to hydrodynamic coupling. In contrast, atomic particles move without friction, and the dynamics are correctly represented with Newton's equations of motion. Nevertheless, as already indicated, it is found that the overall behavior of the single-particle mean squared displacement determined from molecular dynamics simulations is the same as that observed in a real quasi-two-dimensional colloid assembly.

The principal difference between the use of Newtonian mechanics in a molecular dynamics simulation and Langevin mechanics in a Brownian dynamics simulation is associated with high-frequency motions. In particular, the random force that

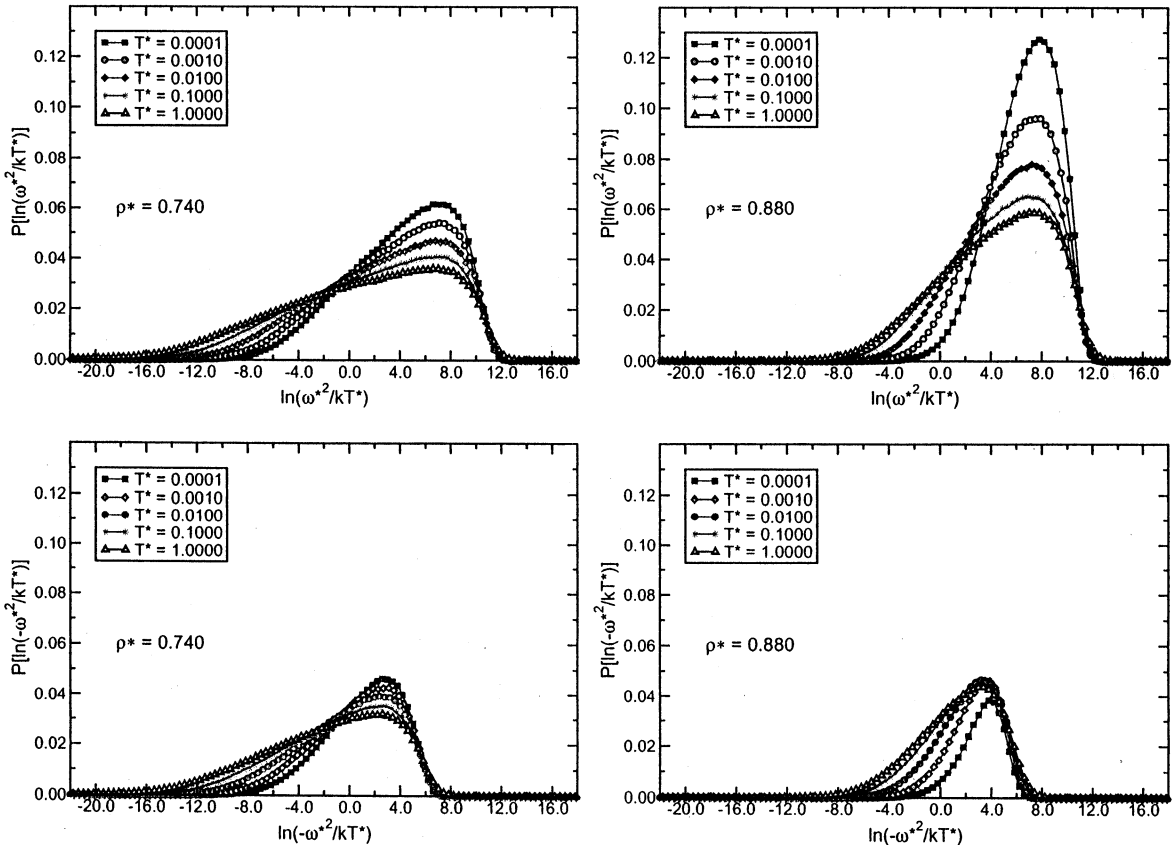

Figure 15. Distribution of the natural logarithm of the real (upper panel) and imaginary (lower panel) frequencies scaled by kT^* in the temperature range $1.0000 \leq T^* \leq 0.0001$ for $\rho^* = 0.740$ and 0.880.

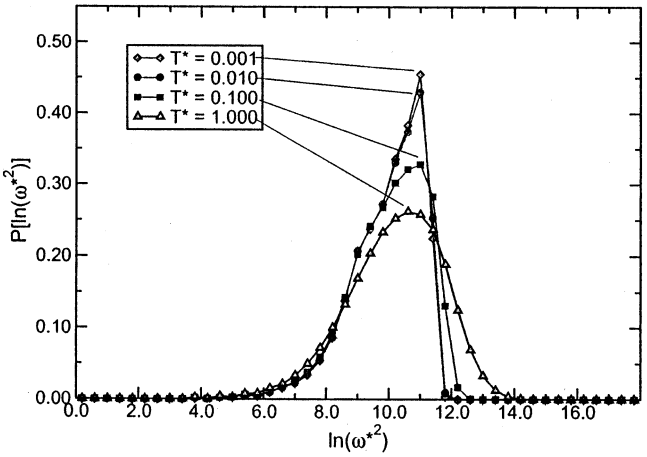

Figure 16. Distribution of the normal mode frequencies for $\rho^* = 1.120$. There are no imaginary frequencies at this high-density solid. Note that in contrast to the behavior at lower densities, the distributions are peaked at around the same frequency for all temperatures.

appears in the Langevin equation of motion in Brownian dynamics simulations has a correlation time that is infinitesimally short, which generates different particle dynamics in the two types of simulations for a time interval that is smaller than the average time between Brownian particle collisions. However, whether the equation of motion has Newtonian or Langevin form, the mean squared displacement of a particle at very short time is a quadratic function of time and at very long time is a linear function of time.[48] The many collisions that occur in the intermediate and long time regimes transform the deterministic behavior of a molecular dynamics simulation to stochastic behavior and, eventually, hydrodynamic flow. It is worth noting that hydrodynamic interactions in quasi-two-dimensional systems are anomalous in a number of respects. These interactions are, in three dimensions, long ranged, thereby generating complicated many-particle effects. However, the confinement of the fluid drastically affects the range and character of the hydrodynamic interactions. In a quasi-one-dimensional system that range is restricted to the channel width.[49] In a quasi-two-dimensional system the hydrodynamic coupling between two particles falls off as r^{-2}, and it has been found that there is a remarkable insensitivity of the large separation behavior of that interaction to changes in particle density.[50] It can be proven that the correction to the pair hydrodynamic interaction due to third particles (i.e., the first-order correction in packing fraction) vanishes. The next order (four-body effect) does not vanish but is expected to be very small. For most practical purposes, therefore, even at high particle concentrations, one may regard the hydrodynamic interaction at large distances in a quasi-two-dimensional system as a long-ranged, yet purely pairwise effect. This surprising result is unique to the quasi-two-dimensional two-plate geometry. It has the consequence that the absence of direct hydrodynamic interactions in the simulation mechanics will not lead to qualitative error. It is for these reasons that the behavior of the mean squared particle displacement in colloid and atomic systems is qualitatively the same.

Returning now to the calculations reported in this paper, the correlated motion of the particles is found to become relatively more important as the density is increased or the temperature is decreased. The continuity of the collective motion from the quasi-two-dimensional liquid phase through the hexatic phase and into the crystalline phase suggests that it has a common physical basis. We suggest identifying that common physical basis as the distribution of instantaneous normal mode frequencies. In particular, it is shown that the time for which the cooperative motion in the system is maximum, t_{max}, is related

to the frequencies of the most populated imaginary normal modes $-\omega^{*2}_{max}$. This behavior is consistent with the argument that the collective motion that is characteristic of a quasi-two-dimensional liquid in the intermediate time regime is generated by superpositions of instantaneous normal mode excitations with free energy greater than the free energy barrier for hopping. As the density increases or the temperature decreases, the lifetimes of the instantaneous normal vibrations increase, thereby allowing more effective competition between cooperative hopping motion and independent particle motion so that the cooperative hopping becomes increasingly dominant. The natural hopping directions are along axes with strong bond-orientation correlation. This mechanism is rather like that proposed for one particle diffusion in crystals. Rice and co-workers showed that the diffusion coefficient can be represented in terms of a superposition of the normal vibrations of the crystal that have nonvanishing projections on the path between an occupied site and a neighboring vacant site.[51−55]

The notion that correlated motion in so-called "cooperatively rearranging regions" defines the dynamics of particle transport in a liquid was first introduced by Adam and Gibbs for the case of dense glass-forming liquids.[56] The typical size of a cooperatively rearranging region grows with decreasing temperature.[4−7] In a more recent development of an alternative theory, Halpern extended the random energy model for three-dimensional supercooled liquids to include two routes for the particles to leave their traps by thermal excitation. The correlated motion of a group of particles was assigned a smaller activation energy and a smaller prefactor (a smaller matrix element for the transition) than independent particle motion so that at low temperature it dominates the diffusion mechanism.[57]

There is a striking similarity between the single-particle displacement distribution in a quasi-two-dimensional liquid near the liquidus with that obtained near the glass transition for glass-forming liquids. However, there is also a fundamental difference between these results. The glass transition is a kinetic effect in the sense that it does not correspond to the global minimum of the free energy of the system; hence, the particle motion near the glass transition will tend to drive the system toward a more stable state. On the other hand, the correlated motion in a quasi-two-dimensional liquid is present in the field of equilibrium states of the system, and both the structural and thermal properties of the system are independent of the time.

Acknowledgment. The research reported in this paper was supported by a Marie Curie Fellowship of the European Community, the Fifth Framework Program, under Contract No. MCFI-1999-00161 and by the National Science Foundation via Grant NSF-CHE 9977841.

References and Notes

(1) Nijboer, B. R. A.; Rahman, A. *Physica* **1966**, *32*, 415−432.
(2) Rahman, A. *Phys. Rev.* **1964**, *136*, A405−A411.
(3) Levesque, D.; Verlet, L. *Phys. Rev. A* **1970**, *2*, 2514−2528.
(4) Kob, W.; Donati, C.; Plimpton, S. J.; Poole, P. H.; Glotzer, S. C. *Phys. Rev. Lett.* **1997**, *79*, 2827−2830.
(5) Donati, C.; Douglas, J. F.; Kob, W.; Plimpton, S. J.; Poole, P. H.; Glotzer, S. C. *Phys. Rev. Lett.* **1998**, *80*, 2338−2341.
(6) Kegel, W. K.; van Blaaderen, A. *Science* **2000**, *287*, 290−293.
(7) Weeks, E. R.; Crocker, J. C.; Levitt, A. C.; Schofield, A.; Weitz, D. A. *Science* **2000**, *287*, 627−631.
(8) Hurley, M. M.; Harrowell, P. *Phys. Rev. E* **1995**, *52*, 1694−1698.
(9) Hurley, M. M.; Harrowell, P. *J. Chem. Phys.* **1996**, *105*, 10521−10526.
(10) Perera, D. N.; Harrowell, P. *J. Chem. Phys.* **1999**, *111*, 5441−5454.
(11) Reichhardt, C.; Reichhardt, C. J. O. *Phys. Rev. Lett.* **2003**, *90*, 095504.
(12) Marcus, A. H.; Schofield, J.; Rice, S. A. *Phys. Rev. E* **1999**, *60*, 5727−5736.
(13) Cui, B.; Lin, B.; Rice, S. A. *J. Chem. Phys.* **2001**, *114*, 9142−9155.
(14) Zangi, R.; Rice, S. A. *Phys. Rev. E* **2003**, *68*, 061508.
(15) Zangi, R.; Rice, S. A. *Phys. Rev. Lett.* **2004**, *92*, 035502.
(16) Born, M.; Huang, K. *The Dynamical Theory of Crystals*; Oxford University Press: Oxford, 1955.
(17) Zwanzig, R. *Phys. Rev.* **1967**, *156*, 190−195.
(18) Keyes, T. *J. Chem. Phys.* **1994**, *101*, 5081−5092.
(19) Keyes, T.; Vijayadamodar, G. V.; Zurcher, U. *J. Chem. Phys.* **1997**, *106*, 4651−4657.
(20) Rahman, A.; Mandell, M. J.; McTague, J. P. *J. Chem. Phys.* **1976**, *64*, 1564−1568.
(21) Cotterill, R. M. J.; Madsen, J. U. *Phys. Rev. B* **1986**, *33*, 262−268.
(22) Rosenberg, R. O.; Thirumalai, D.; Mountain, R. D. *J. Phys.: Condens. Matter* **1989**, *1*, 2109−2114.
(23) Beck, T.; Marchioro, T. L. *J. Chem. Phys.* **1990**, *93*, 1347−1357.
(24) Wallace, D. C.; Clements, B. E. *Phys. Rev. E* **1999**, *59*, 2942−2954.
(25) La Nave, E.; Scala, A.; Starr, F. W.; Sciortino, F.; Stanley, H. E. *Phys. Rev. Lett.* **2000**, *84*, 4605−4608.
(26) Madan, B.; Keyes, T.; Seeley, G. *J. Chem. Phys.* **1990**, *92*, 7565−7569.
(27) Madan, B.; Keyes, T. *J. Chem. Phys.* **1993**, *98*, 3342−3350.
(28) Keyes, T. *J. Phys. Chem. A* **1997**, *101*, 2921−2930.
(29) Adams, J. E.; Stratt, R. M. *J. Chem. Phys.* **1990**, *9S*, 1332−1346.
(30) Buchner, M.; Ladanyi, B. M.; Stratt, R. M. *J. Chem. Phys.* **1992**, *97*, 8522−8535.
(31) Stratt, R. M. *Acc. Chem. Res.* **1995**, *28*, 201−207.
(32) Goldstein, M. *J. Chem. Phys.* **1969**, *51*, 3728−3739.
(33) Zwanzig, R. *J. Chem. Phys.* **1983**, *79*, 4507−4508.
(34) LaViolette, R. A.; Stillinger, F. H. *J. Chem. Phys.* **1985**, *83*, 4079−4085.
(35) Madan, B.; Keyes, T.; Seeley, G. *J. Chem. Phys.* **1991**, *94*, 6762−6769.
(36) Keyes, T. *Phys. Rev. E* **2000**, *62*, 7905−7908.
(37) Seeley, G.; Keyes, T. *J. Chem. Phys.* **1989**, *91*, 5581−5586.
(38) Seeley, G.; Keyes, T.; Madan, B. *J. Chem. Phys.* **1991**, *95*, 3847−3849.
(39) Sciortino, F.; Tartaglia, P. *Phys. Rev. Lett.* **1997**, *78*, 2385−2388.
(40) Li, W.-X.; Keyes, T. *J. Chem. Phys.* **1997**, *107*, 7275−7277.
(41) Donati, C.; Sciortino, F.; Tartaglia, P. *Phys. Rev. Lett.* **2000**, *85*, 1464−1467.
(42) Chowdhary, J.; Keyes, T. *Physica A* **2002**, *314*, 575−582.
(43) Adams, J. E.; Stratt, R. M. *J. Chem. Phys.* **1990**, *93*, 1632−1640.
(44) Zangi, R.; Rice, S. A. *Phys. Rev. E* **1998**, *58*, 7529−7544.
(45) Verlet, L. *Phys. Rev.* **1967**, *159*, 98−103.
(46) Swope, W. C.; Andersen, H. C.; Berens, P. H.; Wilson, K. R. *J. Chem. Phys.* **1982**, *76*, 637−649.
(47) Preparata, F. P.; Shamos, M. I. *Computational Geometry, An Introduction*; Springer-Verlag: New York, 1985.
(48) Hansen, J. P.; McDonald, I. R. *Theory of Simple Liquids*, 2nd ed.; Academic Press: London, 1986.
(49) Cui, B.; Diamant, H.; Lin, B. *Phys. Rev. Lett.* **2002**, *89*, 188302.
(50) Cui, B.; Diamant, H.; Lin, B.; Rice, S. A. *Phys. Rev. Lett.*, in press.
(51) Rice, S. A. *Phys. Rev.* **1958**, *112*, 804−811.
(52) Rice, S. A.; Nachtrieb, N. H. *J. Chem. Phys.* **1959**, *31*, 139−145.
(53) Manley, O. P.; Rice, S. A. *Phys. Rev.* **1960**, *117*, 632−634.
(54) Lawson, A. W.; Rice, S. A.; Corneliussen, R. D.; Nachtrieb, N. H. *J. Chem. Phys.* **1960**, *32*, 447−455.
(55) Rice, S. A.; Frisch, H. L. *J. Chem. Phys.* **1960**, *32*, 1026−1034.
(56) Adam, G.; Gibbs, J. H. *J. Chem. Phys.* **1965**, *43*, 139−146.
(57) Halpern, V. *Philos. Mag. B* **2001**, *81*, 1237−1247.